

A Lagrangian Approach to Modelling Proppant Transport with Tip Screen-Out in KGD Hydraulic Fractures

E. V. Dontsov¹ · A. P. Peirce²

Received: 25 August 2015 / Accepted: 28 August 2015
© Springer-Verlag Wien 2015

Abstract This study introduces a continuum approach to model proppant transport in hydraulic fractures in a Lagrangian frame of reference. The model for the proppant transport is based on the recently obtained slurry flow solution inside a channel, where the latter utilizes a phenomenological constitutive relationship for a slurry. This approach allows us to describe the transition from Poiseuille flow with an effective viscosity to Darcy flow as the particle concentration increases towards the maximum value. The algorithm is presented for the one-dimensional case, for which propagation of a symmetric Kristinovich–Zhel'tov–Geertsma–De Klerk fracture is considered. To examine the effectiveness of the Lagrangian approach for proppant transport modelling, a set of parameters, for which proppant particles reach the fracture tip and cause the development of a proppant plug is selected. In this situation, the coupling between the hydraulic fracture propagation and proppant transport is the most significant. To estimate the accuracy of the Lagrangian proppant transport model, the results are compared to the predictions of an Eulerian proppant transport model, which utilizes the same algorithm for hydraulic fracture propagation. It is shown that, although both approaches have the same convergence rate, the error of the Lagrangian approach is three to five times smaller, which depends on the number of proppant elements used in the Lagrangian approach. This permits us to use a coarser mesh for hydraulic fracture

propagation, and to obtain results with similar accuracy up to a hundred times faster.

Keywords Hydraulic fracturing · Proppant transport · KGD fractures

List of Symbols

t	Time
z	Spatial coordinate
w	Fracture width
l	Fracture half-length
Q_0	Inlet flux
$\bar{\phi}_0$	Inlet normalized proppant concentration
q_z^s	Slurry flux in the z direction
q_z^p	Proppant flux in the z direction
$\bar{\phi}$	Normalized proppant concentration
C'	Scaled leak-off coefficient
$t_0(z)$	Time at which a fracture front is located at point z
μ'	Scaled fluid viscosity
p	Fluid pressure
a	Proppant radius
E'	Plane strain Young's modulus
K'	Scaled fracture toughness
V	Fracture velocity of propagation
ζ	Scaled spatial coordinate
\mathcal{V}_k	Volume of the proppant element

✉ E. V. Dontsov
edontsov@central.uh.edu

A. P. Peirce
peirce@math.ubc.ca

¹ University of Houston, Houston, TX, USA

² University of British Columbia, Vancouver, BC, Canada

1 Introduction

Hydraulic fracturing is a commonly used technique to stimulate oil and gas wells Economides and Nolte (2000). To prevent a fracture from closing after treatment, propping agents, such as sand or ceramic proppants are pumped

along with the fracturing fluid at some stage. To design a fracturing treatment, it is important to know when the proppant should be added, where the proppant goes, and how the proppant affects the fracture propagation. The first issue is related to proppant scheduling, which is analyzed in Nolte (1986), Gu and Desroches (2003) and Dontsov and Peirce (2014b). While the second and the third problems address the proppant transport phenomenon, which is discussed below.

The phenomenon of proppant transport has been studied from both modelling and experimental points of view - Daneshy (1978), Mobbs and Hammond (2001) and Shokir and Al-Quraishi (2007). Often, the problem of proppant transport is not coupled to the hydraulic fracture propagation and mainly gravitational settling is analyzed. In other words, proppant transport and settling in a pre-existing fracture cavity is considered, see e.g. Mobbs and Hammond (2001). Many studies address the problem of flow of a viscous fluid mixed with spherical particles in a channel Eskin and Miller (2008) and Lecampion and Garagash (2014), but do not also consider the coupled problem. One possible technique for coupling hydraulic fracture propagation and proppant transport is described in Adachi et al. (2007). In that approach it is assumed that the proppant concentration changes the fluid viscosity according to a given law, while the proppant transport is described using a convection equation. A more sophisticated model for a one-dimensional problem is proposed in Chekhonin and Levonyan (2012), where the effect of tip screen-out is considered. In Chekhonin and Levonyan (2012), the fracture is divided into two zones: (1) the convection zone, in which the slurry flow behaves according to Poiseuille's law with an effective viscosity, and (2) the plug zone (i.e. packed proppant), where the fluid permeates through the plug according to Darcy's law. One of the biggest drawbacks of this model, however, is its inapplicability to planar fractures.

The proppant transport model that is used for this study, is developed in Dontsov and Peirce (2014c). The model is based on a steady solution for slurry flow in a channel, which is obtained using the phenomenological constitutive relation proposed in Boyer et al. (2011). The constitutive model assumes that the slurry consists of a viscous fluid mixed with spherical particles, while the maximum proppant concentration is determined as $\phi_m = 0.585$. Since a continuum description is used, it is also assumed that the particle size is significantly smaller than the fracture width. Finally, since a steady solution is used to formulate the proppant transport problem, the behaviour in the regions where transient effects are substantial, such as near the clear fluid pad/slurry interface, is not captured accurately. One of the biggest advantages of the considered proppant transport model lies in the fact that it captures the transition

from Poiseuille's law with an effective viscosity to Darcy's filtration law automatically without considering two different zones explicitly, where the values of the effective viscosity and permeability appear naturally from the adopted phenomenological constitutive law. The aforementioned proppant transport model is implemented in Dontsov and Peirce (2015) for Kristinovich–Zhel'tov–Geertsma–De Klerk (KGD) and pseudo-3D fractures, where the governing equations for both hydraulic fracture propagation and proppant transport are solved in an Eulerian frame of reference. Unfortunately, in situations when the proppant has reached the fracture tip and has developed a plug, the predictions for the fracture length and borehole pressure, calculated using the Eulerian scheme, featured visible oscillations even for a relatively fine mesh. This is better illustrated in Dontsov and Peirce (2014a), where the effect of proppant size on the hydraulic fracture propagation is studied. It should be noted, that these oscillations are caused by the numerical scheme, and to suppress them, a very fine mesh should be used. The use of a very fine mesh, however, leads to unnecessary computational costs associated with the propagation of a hydraulic fracture, which reduces the overall efficiency of the approach.

To address the issue of poor accuracy of the Eulerian-based numerical scheme at nearly maximum proppant concentrations, this study aims to introduce an alternative method based on a Lagrangian approach. It should be noted here that by the "Lagrangian approach", we mean the solution of the governing equations on the continuum level in a Lagrangian frame of reference. This is different from the Lagrangian approach used in Patankar (2001), where the motion of each particle is simulated. At the same time, there are some similarities with the studies Andrews and O'Rourke (1996) and Healy and Young (2005), where a Lagrangian approach is used to track particles in a multi-phase flow. The use of a Lagrangian frame of reference for this study, however, is inspired by Dontsov and Peirce (2014b), where such an approach was successfully applied to generate a proppant schedule. One of the biggest advantages of using a Lagrangian frame of reference from the numerical point of view lies in the fact that the grid points associated with the proppant are independent of the corresponding mesh that is used for the hydraulic fracture propagation. This permits us to use a relatively coarse mesh for the hydraulic fracture propagation part, and a finer mesh for the proppant transport. To evaluate the accuracy of the Lagrangian approach, this study aims to consider a simple case of a KGD fracture. Firstly, Sect. 2 describes the governing equations for a hydraulic fracture propagating with proppant transport. Secondly, Sect. 3 describes the equations for proppant transport written in a Lagrangian frame of reference. Section 4 presents the details of the numerical scheme. Section 5 compares model

predictions that are based on the Eulerian and Lagrangian approaches, while Sect. 6 summarizes the results.

2 KGD Hydraulic Fracturing Model with Proppant Transport

This section describes a mathematical model for a one-dimensional KGD hydraulic fracture generated by a slurry. With reference to Fig. 1, it is assumed that the fracture propagates along the z -axis, where the origin represents the location of the wellbore. Considering only symmetric fractures for simplicity, the fracture half-length is denoted by l , in which case the left fracture tip is located at $-l$, while the right fracture tip is located at l . Following Dontsov and Peirce (2014c), the balance laws describing the fracture propagation and the proppant transport can be written as

$$\begin{aligned} \frac{\partial w}{\partial t} + \frac{\partial q_z^s}{\partial z} + \frac{C'}{\sqrt{t-t_0(z)}} &= Q_0 \delta(z), \\ \frac{\partial w \bar{\phi}}{\partial t} + \frac{\partial q_z^p}{\partial z} &= \bar{\phi}_0 Q_0 \delta(z), \end{aligned} \tag{1}$$

where w denotes the fracture opening, $C' = 2C_L$ [C_L is Carter’s leak-off coefficient Carter (1957)], $t_0(z)$ is the time at which the fracture front was located at point z , Q_0 is the injection volume of the slurry per unit time per unit length in the out-of-plane direction, $\bar{\phi}$ is the normalized proppant concentration $0 \leq \bar{\phi} \leq 1$ ($\bar{\phi} = \phi/\phi_m$, so that $\bar{\phi} = 1$ corresponds to the maximum concentration $\phi_m = 0.585$), $\bar{\phi}_0$ is the normalized input proppant concentration. Here the slurry and proppant fluxes are given by

$$\begin{aligned} q_z^s &= -\frac{w^3}{\mu'} \hat{Q}^s\left(\bar{\phi}, \frac{w}{a}\right) \frac{\partial p}{\partial z}, \\ q_z^p &= B\left(\frac{w}{a}\right) \hat{Q}^p\left(\bar{\phi}, \frac{w}{a}\right) q_z^s, \end{aligned} \tag{2}$$

where $\mu' = 12\mu^f$ is the scaled viscosity, p denotes the fluid pressure, while a is proppant radius. It is noted that the gravitational settling is not included in (2) to simplify the analysis. The blocking function B is introduced to describe proppant bridging, where the latter occurs when the fracture width becomes smaller than several particle diameters.

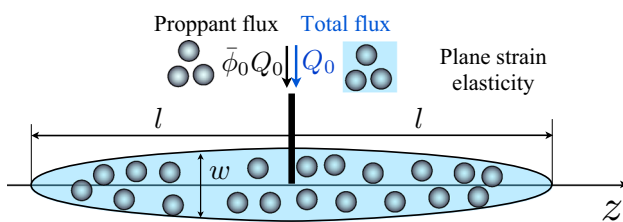


Fig. 1 Schematics of a KGD fracture with proppant

The blocking function B forces the proppant flux to vanish gradually when the fracture width becomes sufficiently small. For the purpose of efficient numerical calculations, the blocking function is approximated by a smooth function

$$\begin{aligned} B\left(\frac{w}{a}\right) &= \frac{1}{2} H\left(\frac{w}{2a} - N\right) H\left(\frac{w_B - w}{2a}\right) \\ &\times \left[1 + \cos\left(\pi \frac{w_B - w}{2a}\right) \right] + H\left(\frac{w - w_B}{2a}\right). \end{aligned} \tag{3}$$

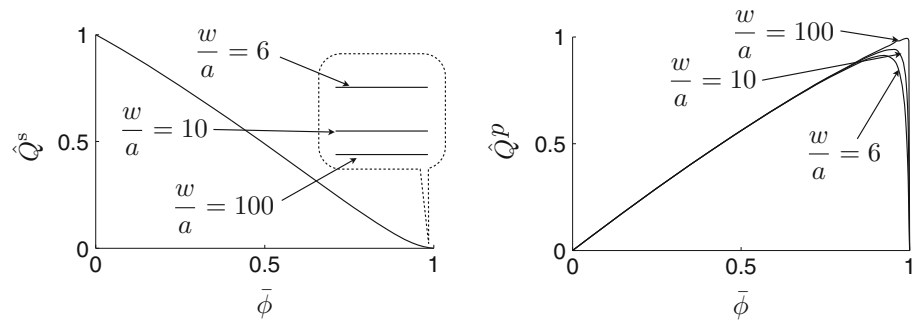
Here H is Heaviside step function, $w_B = 2a(N+1)$, while $N = 3$ represents the number of particle diameters needed to cause proppant bridging. This number ($N = 3$) is consistent with the experimental study Gruesbeck and Collins (1982), which shows that proppant particles develop a bridge in a perforation when the perforation diameter is between two to six particle diameters.

Functions \hat{Q}^s , \hat{Q}^p that appear in (2) play a crucial role in the model, as they describe the influence of the particles on the slurry flux (and consequently on the fracture propagation), and conversely the influence of the fracture propagation on the proppant transport. According to Dontsov and Peirce (2014c), the aforementioned functions can be written as

$$\begin{aligned} \hat{Q}^s\left(\bar{\phi}, \frac{w}{a}\right) &= Q^s(\bar{\phi}) + \frac{a^2}{w^2} \bar{\phi} D, \\ \hat{Q}^p\left(\bar{\phi}, \frac{w}{a}\right) &= \frac{Q^p(\bar{\phi})}{\hat{Q}^s\left(\bar{\phi}, \frac{w}{a}\right)}, \end{aligned} \tag{4}$$

where Q^s and Q^p are functions of $\bar{\phi}$ only and are calculated numerically, $D = 8(1 - \phi_m)^{\bar{\alpha}} / (3\phi_m)$ is related to the permeability of the packed particles, where $\phi_m = 0.585$ is the volume fraction of the packed particles, and $\bar{\alpha} = 4.1$, see Davis and Acrivos (1985). Figure 2 shows the functions \hat{Q}^s and \hat{Q}^p versus normalized proppant concentration $\bar{\phi}$ for different values of the parameter w/a . The function $Q^s(\bar{\phi})$ in the first equation in (4) is the reciprocal of the effective slurry viscosity and determines the behaviour for almost all values of $\bar{\phi}$, except $\bar{\phi} \approx 1$. The second term featuring D becomes important only for $\bar{\phi} \approx 1$ and describes fluid filtration through the packed proppant (i.e. Darcy’s law). So, the slurry flux in (2) is capable of capturing the transition from Poiseuille flow (featuring effective viscosity) to Darcy flow as the concentration increases from small to nearly the maximum value. As can be seen from Fig. 2, the function \hat{Q}^p in the proppant flux in (2) is proportional to $\bar{\phi}$ at low concentrations, while it decreases sharply to zero for $\bar{\phi} \approx 1$. This decrease is due to the fact that the proppant forms an immobile plug when the concentration reaches the maximum value ($\bar{\phi} = 1$), while the fluid can still move through the plug by filtration. It should be noted here, that the proppant transport model introduced

Fig. 2 Functions \hat{Q}^s and \hat{Q}^p featured in the model (4) versus the normalized proppant concentration $\bar{\phi}$ for different values of the parameter w/a



in Dontsov and Peirce (2014c) is closely related to the one in Lecampion and Garagash (2014). In particular, both approaches are based on the phenomenological constitutive model for slurry Boyer et al. (2011). The model in Lecampion and Garagash (2014), however, neglects the slip velocity between the two phases from the outset, and, as a result, lacks the Darcy-related term in (4). The latter term plays a crucial role in situations when the crack tip screen-out is present, which is considered in this study. More detailed comparison between two models can be found in Dontsov and Peirce (2014c).

To close the system of equations (1), the fluid pressure is determined using the elasticity equation, which ensures that the rock that surrounds the fracture is in equilibrium, namely

$$p = -\frac{E'}{4\pi} \int_{-l}^l \frac{w ds}{(s-z)^2}. \quad (5)$$

Here the elastic interactions are calculated assuming plane strain conditions, $E' = E/(1-\nu^2)$ denotes the corresponding plane strain Young's modulus, and the integral is understood in the sense of a Hadamard finite part. Finally, the boundary and propagation conditions at the fracture tip can be written as

$$q_z^s|_{z=l} = 0, \quad w \rightarrow \frac{K'}{E'}(l-z)^{1/2}, \quad z \rightarrow l, \quad (6)$$

where $K' = 8K_{Ic}/\sqrt{2\pi}$ is the scaled fracture toughness. Note that there is no need to prescribe a zero proppant flux boundary condition, as it is satisfied automatically since the blocking functions preclude proppant from entering the tip region.

3 Lagrangian Description of the Proppant Transport

The equations that govern hydraulic fracture propagation and proppant transport that are outlined in the previous section are written inherently in an Eulerian frame of

reference. These equations were solved numerically in Dontsov and Peirce (2015). However, the numerical scheme for solving the proppant transport problem is cumbersome and not computationally efficient. In particular, the computational error becomes visible even if a fine mesh is used in situations when a proppant plug is formed, see Dontsov and Peirce (2014a). In addition, the mesh for the proppant is tied to the fracture opening grid that is used to discretize (1). In this situation, if one needs better accuracy (i.e. a finer mesh) for the proppant placement, one has to use the same fine mesh for the fracture width calculations, which substantially increases the computational time. To overcome these disadvantages, this study suggests an alternative approach, where a Lagrangian frame of reference is used to solve for the proppant motion inside the fracture.

To rewrite the problem of proppant transport in a Lagrangian frame of reference, it is useful to integrate the second equation in (1) in space over the interval $(z_1(t), z_2(t))$. This yields

$$\frac{d}{dt} \int_{z_1(t)}^{z_2(t)} w \bar{\phi} dz - (w \bar{\phi})|_{z_2} \frac{dz_2}{dt} + (w \bar{\phi})|_{z_1} \frac{dz_1}{dt} + q_z^p|_{z_2} - q_z^p|_{z_1} = \bar{\phi}_0 Q_0 (H(z_2) - H(z_1)), \quad (7)$$

where H is the Heaviside step function. To preserve the total amount of proppant in the interval $(z_1(t), z_2(t))$, one should require

$$\frac{dz_i}{dt} = \frac{q_z^p}{w \bar{\phi}}|_{z_i} \equiv V_z^p(w(z_i), \bar{\phi}(z_i)), \quad i = 1, 2, \quad (8)$$

where $V_z^p(w(z_i), \bar{\phi}(z_i))$ is the proppant velocity at point z_i . Accordingly, Eq. (7) reduces to

$$\frac{d}{dt} \int_{z_1(t)}^{z_2(t)} w \bar{\phi} dz = \bar{\phi}_0 Q_0 (H(z_2) - H(z_1)). \quad (9)$$

Equations (8) and (9) form the basis for the numerical calculation of proppant transport in a Lagrangian frame of reference. Equation (8) allows us to track proppant particles in space, while the volume balance Eq. (9) can be used to determine the particle concentration at a given point in

space. Note that since $\hat{Q}^p \propto \bar{\phi}$ for small values of $\bar{\phi}$ (see Fig. 2), the proppant velocity defined in (8) does not have a singularity.

4 Numerical Scheme

This section outlines the numerical algorithm for solving the propagation of a KGD fracture induced by a slurry, where proppant transport is calculated using a Lagrangian approach. At each time step, the numerical scheme performs two procedures: (a) an incremental solution for the fracture propagation for a given proppant concentration, and (b) an incremental solution for the proppant motion using the fracture movement determined previously in (a). Note that the first step is the same as in Dontsov and Peirce (2015), while the second step is fundamentally different.

First, let us briefly describe algorithm used to calculate fracture propagation. To facilitate the numerical solution of the moving boundary problem under consideration, the spatial coordinate z is replaced by $\zeta = z/l(t)$, $0 \leq \zeta \leq 1$. In this case, the first equation in (1) can be rewritten as

$$\frac{\partial w}{\partial t} - \frac{V}{l} \zeta \frac{\partial w}{\partial \zeta} + \frac{1}{l} \frac{\partial q_z^s}{\partial \zeta} + \frac{C'}{\sqrt{t-t_0(l\zeta)}} = \frac{Q_0}{l} \delta(\zeta), \tag{10}$$

where $V = dl/dt$ is the velocity of crack propagation. To solve (10) numerically, ζ is discretized using a uniform grid, and the fracture width is approximated by a piece-wise constant function, defined by its values at the nodes of ζ_i , $i = 1, \dots, N_z$. To advance the fracture from time instant t_1 to t_2 , Eq. (10) is discretized as

$$\begin{aligned} \frac{w_i - w_i^0}{t_2 - t_1} - \frac{V}{l} \zeta_i \frac{w_{i+1} - w_{i-1}}{2\Delta\zeta} + \frac{1}{l} \frac{q_{z,i+1/2}^s - q_{z,i-1/2}^s}{\Delta\zeta} \\ + 2C' \frac{\sqrt{t_2 - t_0(l\zeta_i)} - \sqrt{t_1 - t_0(l\zeta_i)}}{t_2 - t_1} = \frac{Q_0}{l\Delta\zeta} \delta_{i1}, \end{aligned} \tag{11}$$

where w_i denotes the fracture opening at ζ_i at time instant t_2 , while w_i^0 denotes the fracture opening at the previous time step, which corresponds to the time instant t_1 . Here δ_{i1} is the Kronecker delta, which ensures that the source belongs exclusively to the first element. The slurry flux in (11) is discretized as

$$q_{z,i+1/2}^s = -\frac{w_{i+1/2}^3}{\mu'} \hat{Q}^s \left(\bar{\phi}_{i+1/2}, \frac{w_{i+1/2}}{a} \right) \frac{p_{i+1} - p_i}{l\Delta\zeta}. \tag{12}$$

The latter equation features proppant concentration at the midpoints $\bar{\phi}_{i+1/2}$, which is assumed to be known. The fluid pressure that enters (12) is calculated from the displacement discontinuity Eq. (5) assuming piece-wise constant fracture widths. In particular

$$\begin{aligned} p_i = \frac{E'}{4\pi l} \left(\sum_{j=1}^{N_z} w_j \left[\frac{1}{(\zeta_j + \frac{1}{2}\Delta\zeta - \zeta_i)} - \frac{1}{\zeta_j - \frac{1}{2}\Delta\zeta - \zeta_i} \right] \right. \\ \left. + \sum_{j=2}^{N_z} w_j \left[\frac{1}{(-\zeta_j + \frac{1}{2}\Delta\zeta - \zeta_i)} - \frac{1}{-\zeta_j - \frac{1}{2}\Delta\zeta - \zeta_i} \right] \right). \end{aligned} \tag{13}$$

Since the displacement discontinuity method has poor accuracy for the tip element, the pressure at the tip is taken as an unknown. To compensate for this, the fracture propagation velocity, V , is determined assuming that the last element follows the appropriate asymptotic solution, see e.g. Peirce and Detournay (2008) in which this approach is described. Given the fracture velocity, the zero-flux boundary condition in (6) is used to find the pressure at the tip element. With the use of the appropriate asymptotic solution and Eqs. (12) and (13), the nonlinear system of equations (11) is solved iteratively for every time step. Once (11) has been solved, the fracture length is updated using $l = l^0 + V(t_2 - t_1)$. A more detailed description of the fracture propagation algorithm can be found in Dontsov and Peirce (2015).

To describe proppant transport using a Lagrangian approach, proppant elements are introduced. Let us denote the boundaries of the proppant elements by z_k , $k = 1, \dots, N_p + 1$, where N_p is current number of proppant elements and $z_{N_p+1} = 0$. Note that the numbering starts with the proppant elements closest to the tip and ends at the source element, since this is the order in which they are created. In this case, the k th element is located between z_{k+1} and z_k , see Fig. 3. Each proppant element has the associated proppant volume, defined as

$$V_k = \int_{z_{k+1}}^{z_k} w \bar{\phi} dz. \tag{14}$$

According to Eq. (9), this proppant volume is conserved for all elements except the one near the wellbore, which is assumed to be partially filled and denoted by the red rectangle in Fig. 3. For the partially filled element, one has

$$\frac{dV_{N_p}}{dt} = \frac{1}{2} \bar{\phi}_0 Q_0, \tag{15}$$

where the 1/2 factor comes from the symmetry considerations. Equation (15) determines the evolution of the proppant volume for the partially filled element. As soon as the volume reaches some critical value, a new element is introduced, which increases N_p by one. This is the procedure for introducing new proppant elements. In this case, the total number of proppant elements is controlled by the value of that critical proppant volume. Note that the volume is conserved for all elements that are away from the source, and its value is determined by the volume of the

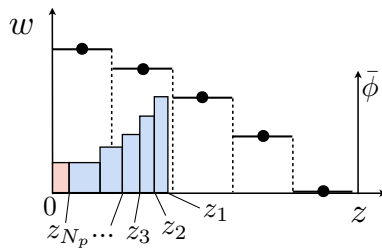


Fig. 3 Schematics of the discretized fracture opening (black lines with dots) and proppant elements (blue-coloured rectangles), where the red rectangle corresponds to partially filled element

partially filled element after it “detaches” from the source. Given the proppant volume for each element, the corresponding elemental proppant concentration can be approximated from (14) using the midpoint rule:

$$\bar{\phi}_k = \frac{V_k}{(z_{k+1} - z_k)w((z_{k+1} + z_k)/2)}. \quad (16)$$

Here $\bar{\phi}_k$ is the normalized proppant concentration for the k th element, while $w((z_{k+1} + z_k)/2)$ is the fracture opening at the center of the element, which is obtained by interpolating between the values of the discretized fracture opening w_i , $i = 1, \dots, N_x$. To evolve the boundaries of the elements, one may employ Eq. (8) to write

$$\frac{dz_k}{dt} = V_z^p(w(z_k), \bar{\phi}(z_k)). \quad (17)$$

Here the proppant velocity V_z^p varies with space through the variations of both, the fracture opening, and the proppant concentration, see (2) and (8). The fracture opening $w(z_k)$ at the point z_k is determined using cubic Hermite interpolation of the discretized fracture opening w_i , $i = 1, \dots, N_x$. To have a stable solution, the proppant concentration, on the other hand, is calculated by allocating the concentration as follows:

$$\bar{\phi}(z_k) = \begin{cases} \bar{\phi}_{k-1}, & V_z^p \geq 0, \\ \bar{\phi}_k, & V_z^p < 0. \end{cases} \quad (18)$$

To stabilize Eulerian discretizations upwinding is typically required. The analogue for the Lagrangian scheme is that it is necessary to ensure that the velocity of a proppant element boundary depends on the proppant concentration in the element towards which this node will move. Thus, the Eq. (18) suggests that the proppant concentration is determined by the element ahead of the corresponding node z_k if $V_z^p \geq 0$, and by the element behind if $V_z^p < 0$. Zero concentration is taken for the first element if $V_z^p \geq 0$, since there is a clear fluid ahead of it, see Fig. 3. Note that the sign of V_z^p is solely determined by q_z^s , which is pre-computed during calculation of the fracture propagation. Also note that the values of q_z^s are fixed during the

calculation of proppant motion via (17). In the numerical scheme, a fourth-order Runge–Kutta method is used to solve (17), where each time step corresponding to the fracture propagation was subdivided into smaller time steps to have a stable solution. Note that the fracture propagation step uses the implicit Backward Euler scheme in order that large time steps can be taken. Explicit time stepping of the stiff fracture propagation equations would result in a stability condition requiring $\Delta t \lesssim \Delta z^3$. Once new positions of the elements are calculated, Eq. (16) is used to calculate the normalized proppant concentration within each element. Finally, interpolation is used to determine the values of the proppant concentration at the half-points of the spatial grid, $\bar{\phi}_{i+1/2}$, which are used in (12) for the fracture propagation algorithm. Note that all interpolation is performed using the built-in “PCHIP” function in Matlab, which preserves monotonic behaviour of data.

5 Results and Discussion

To examine the advantages and disadvantages of using the Lagrangian approach to model proppant transport, this section compares the results obtained using the Eulerian and Lagrangian approaches for a set of reference problem parameters. This set of reference parameters is chosen as: $E' = 20$ GPa for the plane strain Young’s modulus, $K_{Ic} = 0$ for the fracture toughness, $\mu' = 1.2$ Pa·s for the fluid viscosity, $C' = 3 \times 10^{-5}$ m/s^{1/2} for the leak-off coefficient, and $Q_0 = 5 \times 10^{-4}$ m²/s for the inlet flux. Firstly, a clear fluid is pumped until $t_{pr} = 1000$ s. Thereafter, a slurry containing proppant particles with normalized concentration $\bar{\phi}_0 = 0.2$ is used. The particle radius is chosen as $a = 0.6$ mm. All simulations are performed until $t_{end} = 10,000$ s. Different mesh sizes are considered, namely $N_z = \{25, 50, 100, 200, 400\}$, where N_z is the number of points in the discretization of the fracture width. In the Eulerian approach, the number of discretization points that corresponds to proppant is $N_z - 1$ (note that the values of the proppant concentration are defined at the midpoints). While in the Lagrangian approach, the largest number of proppant elements is taken as either N_z , $2N_z$, or $4N_z$, which is adjusted using different values of the critical volume for proppant elements. To accommodate a finer mesh, the time step was refined proportionally to the spatial discretization.

Figure 4 shows the evolution of the fracture by plotting the fracture opening at $t = 1500$ s, $t = 2000$ s, $t = 4000$ s, and $t = 10,000$ s. Colour filling indicates normalized proppant concentration. At time $t = 1500$ s the proppant has not yet reached the fracture tip, in which case there is no visible influence on the fracture shape. At $t = 2000$ s, the proppant concentration grows to nearly the maximum

value due to bridging, where the latter is modelled by the blocking function (3). This indicates the initiation of the proppant plug (i.e. the zone where the proppant concentration is nearly maximal). There is no visible influence on the fracture shape at this point. Note that proppant particles reach the fracture tip rapidly due to the leak-off. At $t=4000$ s, however, there is a well-developed proppant plug, and a noticeable change in the fracture shape. Finally, at $t=10,000$ s, the fracture becomes much wider, and the proppant plug increases in size. Note, however, that even with the presence of the proppant plug, there is still some fracture growth between $t=4000$ s and $t=10,000$ s.

To quantify the accuracy of both the Eulerian and Lagrangian approaches, Fig. 5 compares the fracture half-length histories for different meshes $N_z=25$, $N_z=50$, and $N_z=400$. Blue lines correspond to the case for which proppant transport is calculated using the Eulerian approach. Magenta, red, and black lines indicate the results obtained using the Lagrangian proppant transport with N_z , $2N_z$, and $4N_z$ proppant elements, respectively. It is clear that the Eulerian approach becomes inaccurate (for relatively coarse meshes) once the proppant particles have developed a plug after $t \approx 2000$ s. The fracture exhibits stop-and-go behaviour, which causes the oscillations in the fracture length history. For finer meshes, however, the oscillations reduce their magnitude, and almost disappear for $N_z=400$. On the other hand, the Lagrangian approach produces smoother fracture growth even for coarse meshes, especially if more proppant elements are used. To quantify the discrepancy, an error measure is defined as

$$\text{Error} = \sqrt{\frac{\int_0^{t_{\text{end}}} (l(t) - l_{\text{ex}}(t))^2 dt}{\int_0^{t_{\text{end}}} l_{\text{ex}}(t)^2 dt}}, \quad (19)$$

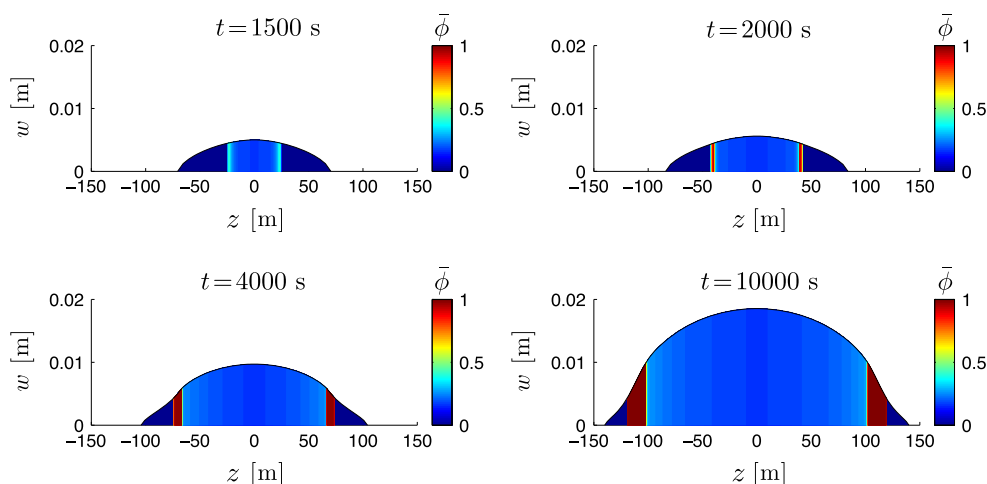
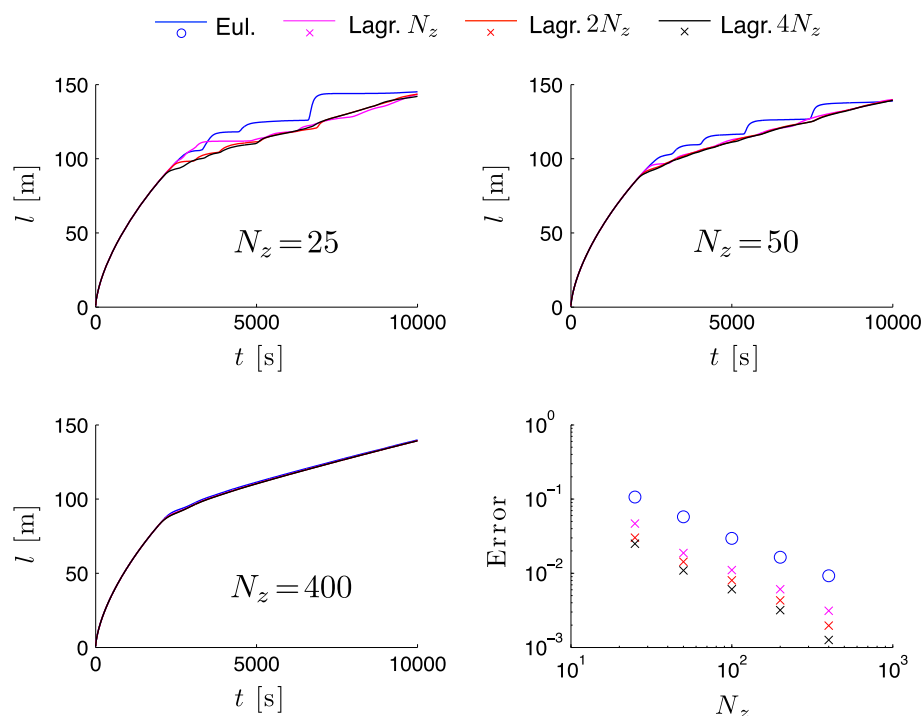


Fig. 4 Fracture opening variation versus spatial coordinate z at different time instants $t = \{1500, 2000, 4000, 10,000\}$ s, calculated for a reference set of parameters. Colour filling indicates normalized proppant concentration

where $l(t)$ is the fracture length history, as shown in Fig. 5, while $l_{\text{ex}}(t)$ corresponds to the length history of the “exact” solution. Here the “exact” solution is calculated using the Lagrangian approach with $N_z=800$ spatial points in the fracture width discretization and $4N_z$ proppant elements. The bottom right picture in Fig. 5 shows the error calculated using (19) for the Eulerian and Lagrangian approaches, where three variations of the latter (with N_z , $2N_z$, and $4N_z$ proppant elements) are considered. One can observe from the figure that all methods converge as N_z increases. Moreover, the convergence rate is approximately equal to one for all cases. This is consistent with the fact that $\Delta t \propto \Delta z$, the fact that the backward Euler time stepping scheme is first-order accurate, and that the piece-wise constant approximation used to discretize the elasticity equation is first-order accurate. It should also be noted that the points that correspond to $N_z=400$ for the Lagrangian approach are slightly shifted downwards since the “exact” solution is not actually exact. Nevertheless, the fracture length calculated using the Lagrangian approach is consistently more accurate for all mesh sizes. Also, the accuracy can be noticeably increased using more proppant elements. Since the number of time steps is taken to be proportional to the number of spatial points, the computational time grows as N_z^3 [note that N_z^2 operations are required to calculate the pressure via (13)]. Since both proppant transport algorithms require $O(N_z^2)$ operations, the type of algorithm and the number of proppant elements have little influence on the computational time. Since the Lagrangian approach reduces the error by factors from three to five depending on the number of proppant elements used (see Fig. 5), one may use a coarser mesh and obtain results with similar accuracy (and no stop-and-go behaviour) up to a hundred times faster.

Fig. 5 Fracture half-length histories calculated using different mesh sizes with $N_z = 25$, $N_z = 50$, and $N_z = 400$ and different algorithms for proppant transport. *Blue lines* indicate results where proppant transport is calculated using the Eulerian approach. *Magenta, red, and black lines* show the results obtained using the Lagrangian approach with N_z , $2N_z$, and $4N_z$ proppant elements, respectively. The *bottom right picture* shows the error calculated using (19) versus mesh size, N_z , for the different approaches



It is very important to emphasize that the error analysis performed in this paper is targeted towards estimation of the discrepancy after the proppant plug formation. The accuracy of calculating the proppant transport before the plug formation is less important because, as can be seen from Fig. 4, there is almost no influence of the proppant on the shape of the fracture before particles form a plug. To verify this hypothesis, the fracture half-length at $t = 1500$ s, $t = 2000$ s and $t = 4000$ s was calculated assuming no proppant and compared to the corresponding results that account for the proppant transport (see Fig. 4 for the proppant distributions inside the fracture at these time instants). The discrepancy of the fracture half-length for $t = 1500$ s is 0.1%, for $t = 2000$ s is 0.6%, while for $t = 4000$ s it is 19.7%. Clearly, the influence of the proppant on fracture propagation is nearly negligible before particles develop a plug. This is because the particles alter the effective fluid viscosity, while the latter becomes important primarily in the regions with large pressure gradients. Since the pressure gradient is large only near the fracture tip, the overall influence of the proppant is small until it reaches the tip region. When the plug is formed, however, the particles cause big a pressure gradient through the plug, which significantly alters further fracture propagation.

The results shown in Fig. 5 demonstrate that the Lagrangian approach for modelling proppant transport is more accurate for KGD fractures than the Eulerian approach. To understand why the Lagrangian approach is

more accurate, let us consider the motion of a developed proppant plug. In the Eulerian approach, the location of the plug is determined up to a precision of one element size. In situations when the fracture widens and the next element becomes “available” for the proppant (i.e. the fracture width becomes larger than 3 particle diameters), the proppant plug moves forward quickly to occupy it. During this process, the proppant plug length increases and the proppant concentration decays within the plug. To compensate the pressure drops through the plug, the fracture starts to grow rapidly. After this fast fracture growth, the leak-off increases substantially, which reduces the fracture width and increases the proppant concentration back in the plug. This causes the fracture to reduce its velocity of propagation or even to stop in the worst case. This is the mechanism for the stop-and-go behaviour observed in Fig. 4. Clearly, this is related to the fact that the front boundary of the proppant plug can only be located at a discrete set of points. On the other hand, in the Lagrangian approach, the proppant elements can be located everywhere along the fracture. This makes the motion of the proppant plug smooth, in which case there are no oscillations in the fracture growth history, which leads to better accuracy. It should be noted here, that a first-order numerical scheme is used to model the proppant transport in the Eulerian approach, see Dontsov and Peirce (2015). Higher order schemes have the potential to mitigate the error, but can be difficult to implement due to the strong coupling between the hydraulic fracture propagation and the proppant

transport in situations when the proppant plug is formed. In addition, since the proppant plug location for a high-order Eulerian scheme is still only accurate up to one element width, it is not clear that the overall gain in the accuracy will be substantial.

It is important to mention that this study considers the simplest case of a symmetric KGD fracture with no stress barriers exclusively to show the effectiveness of the Lagrangian approach. In general, it is possible to include various stress barriers, layers with different fracture toughness, and/or gravitational settling into the model, which are all beyond the scope of this study. In addition, it should be noted that the Lagrangian approach can also be extended to model the proppant transport in fully planar hydraulic fractures. Given the fact that this methodology leads to smooth proppant plug motion, while the Eulerian approach permits proppant plug location only up to one element width, it is expected that the Lagrangian approach will lead to more accurate results for planar fractures too.

The proposed Lagrangian methodology is applied to a particular proppant transport mathematical model, governed by (2)–(4). The numerical scheme, however, is not restricted to this particular model. It is possible to use different functions for \hat{Q}^s and \hat{Q}^p in (4), which can be obtained either from a better model for the slurry flow, or from the experiments.

6 Conclusions

This paper considers the problem of proppant transport in a symmetric KGD fracture. The adopted proppant transport model is based on the slurry flow solution obtained using a phenomenological constitutive relation, where the latter describes the behaviour of a viscous fluid mixed with spherical particles. The main advantage of the selected proppant transport model is that it is able to capture the transition from Poiseuille flow with an effective viscosity to Darcy flow as the particle concentration increases. Equipped with the proppant transport model, this study introduces an alternative approach to solve for the coupled problem of fracture propagation and proppant motion numerically. In particular, the corresponding governing equation for the proppant transport is solved in a Lagrangian frame of reference. The results are then compared to the solution calculated using the same hydraulic fracture simulator but with the proppant transport calculated using an Eulerian approach. A set of problem parameters for which proppant particles reach the fracture tip and develop a plug is considered. For this case, the coupling between the proppant transport and hydraulic fracture propagation is the most significant. It is shown that the hydraulic fracture,

modelled using the Eulerian approach exhibits stop-and-go behaviour once proppant bridging has occurred. This is related to the fact that the front position of the proppant plug can only be located at a discrete set of points, in which case each “jump” of the proppant plug causes rapid fracture growth followed by a time period with almost no growth. In contrast, the use of a Lagrangian approach allows us to have a proppant plug at any location along the fracture, which leads to smooth motion of the plug, and, consequently, smooth fracture growth. Error analysis indicates that the accuracy of the Lagrangian approach is up to an order of magnitude better than that of the Eulerian approach if the same mesh is used. This implies that a coarser mesh can be used to obtain results with similar accuracy, which ultimately leads to faster computations.

Acknowledgments The authors would like to acknowledge the support of the British Columbia Oil and Gas Commission and the NSERC discovery grants program.

References

- Adachi J, Siebrits E, Peirce A, Desroches J (2007) Computer simulation of hydraulic fractures. *Int J Rock Mech Min Sci* 44:739–757
- Andrews MJ, O’Rourke PJ (1996) The multiphase particle-in-cell (MP-PIC) method for dense particulate flows. *Int J Multiph Flow* 22:379–402
- Boyer F, Guazzelli E, Pouliquen O (2011) Unifying suspension and granular rheology. *Phys Rev Lett* 107:188301
- Carter ED (1957) Optimum fluid characteristics for fracture extension. In: Howard GC, Fast CR (eds) *Drilling and production practices*, pp 261–270
- Chekhonin E, Levonyan K (2012) Hydraulic fracture propagation in highly permeable formations, with applications to tip screenout. *Int J Rock Mech Min* 50:19–28
- Daneshy AA (1978) Numerical solution of sand transport in hydraulic fracturing. *J Pet Technol* 132–140
- Davis RH, Acrivos A (1985) Sedimentation of noncolloidal particles at low Reynolds numbers. *Annu Rev Fluid Mech* 17:91–118
- Dontsov EV, Peirce AP (2014a) The effect of proppant size on hydraulic fracturing by a slurry. *Am Rock Mech Assoc*
- Dontsov EV, Peirce AP (2014b) A new technique for proppant schedule design. *Hydraul Fract J* 1(3)
- Dontsov EV, Peirce AP (2014c) Slurry flow, gravitational settling, and a proppant transport model for hydraulic fractures. *J Fluid Mech* 760:567–590
- Dontsov EV, Peirce AP (2015) Proppant transport in hydraulic fracturing: crack tip screen-out in KGD and P3D models. *Int J Solids Struct* 63:206–218
- Economides MJ, Nolte KG (eds) (2000) *Reservoir stimulation*, 3rd edn. Wiley, Chichester
- Eskin D, Miller MJ (2008) A model of non-newtonian slurry flow in a fracture. *Powder Technol* 182:313–322
- Gruesbeck C, Collins RE (1982) Particle transport through perforations. *SPE* 7006(22):857–865
- Gu H, Desroches J (2003) New pump schedule generator for hydraulic fracturing treatment design. In: *SPE Latin American and Caribbean petroleum engineering conference*

-
- Healy DP, Young JB (2005) Full lagrangian methods for calculating particle concentration fields in dilute gas-particle flows. *Proc R Soc A* 461:2197–2225
- Lecampion B, Garagash D (2014) Confined flow of suspensions modeled by a frictional rheology. *J Fluid Mech* 759:197–235
- Mobbs AT, Hammond PS (2001) Computer simulations of proppant transport in a hydraulic fracture. *SPE Prod Facil*, pp 112–121
- Nolte KG (1986) Determination of proppant and fluid schedules from fracturing-pressure decline. *SPE Prod Eng* 255–265
- Patankar NA (2001) Lagrangian numerical simulation of particulate flows. *Int J Multiph Flow* 27:1685–1706
- Peirce A, Detournay E (2008) An implicit level set method for modeling hydraulically driven fractures. *Comput Methods Appl Mech Eng* 197:2858–2885
- Shokir EM, Al-Quraishi AA (2007) Experimental and numerical investigation of proppant placement in hydraulic fractures. In: *SPE Latin American and Caribbean petroleum engineering conference*